Isolated Single-phase AC Grid Connected Converter With small Inductors and Capacitors for Micro-inverters

Hiroki Watanabe
Department of Electrical engineering
Nagaoka University of Technology
Niigata, Japan
hwatanabe@stn.nagaokaut.ac.jp

Jun-ichi Itoh
Department of Electrical engineering
Nagaoka University of Technology
Niigata, Japan
Itoh@vos.nagaokaut.ac.jp

***Abstract*— In this paper, a high power density single-phase inverter for photovoltaic system is presented. The proposed converter consists of a resonance-type isolated DC/DC converter, a power decoupling circuit and a current source inverter (CSI). In particular, the volume reduction of capacitors and inductors is focused. Consequently, a leakage inductor of a center-tapped transformer is used as a DC inductor instead of a large inductor. In addition, the reduction of the input voltage ripple into the DC side without a large smoothing inductor or an electrolytic capacitor is achieved. Finally, the proposed converter also achieves a zero current switching (ZCS) for all switching devices. As a simulation result, the input voltage ripple due to the single-phase power fluctuation is under than 5%, and the total harmonic distortion (THD) of the inverter output current is less than 5%. In addition, the design of the resonance component is discussed. It is observed from the simulation and the experimental result, that the high quality factor Q should be designed in order to achieve the stability of the resonance current.**

Keywords—Photovoltaic; grid connected inverter; active power decoupling; flying capacitor DC-DC converter; single-phase power ripple.

I. INTRODUCTION

Recently, Photovoltaic (PV) system has been researching actively as a sustainable power solution. In order to achieve the flexibility, high system efficiency, and low manufacturing cost, utilization of the micro-inverters may become a trend for future PV system instead of using large capacity inverters [1]-[7]. In particular, the micro-inverter requires the high reliability because many converter units are adopted to the PV system.

In order to satisfy these requirements, many converter topologies have been studied [8]-[10]. In general, the power converter system (PCS) needs the isolation between the PV side and the single-phase AC grid side because the leakage current occurs on the power line and the earth ground. Thus, a non-isolated PCS often requires a bulky isolation transformer with commercial frequency to AC grid side. The micro-inverter system needs many converter units. Thus the commercial frequency isolation transformer increase the system volume.

On the other hand, the micro-inverter with the high frequency transformer such as a fly-back and a resonance-type DC/DC converter has been studying. In particular, resonance-type DC/DC converter achieves a ZCS or Zero voltage Switching (ZVS) utilizing the resonance. However, the converter efficiency decreases in comparison with the non-isolated type converter because of the transformer loss.

In order to eliminate the large electrolytic capacitor, an active power decoupling methods have been studied [11]-[17]. In the DC to single-phase AC grid connection system, the large electrolytic capacitor is required because the instantaneous power fluctuation at the twice grid frequency occurs due to the single-phase AC grid, and it decays the performance of the maximum power point tracking (MPPT). Besides, the electrolytic capacitor limits the life-time of the converter due to the Arrhenius law.

On the other hand, the active power decoupling method can reduce the capacitance for the instantaneous power fluctuation compensation, and a small film or a ceramic capacitor can be used instead of the large electrolytic capacitor. In addition, the elimination of the inductor is important for the high power density design. In particular, the high frequency operation can reduce the inductance greatly. In this case, the reduction of the switching losses is the key technology to achieve both the high efficiency and high power density by the active power decoupling. However, many active power decoupling approach decreases the converter efficiency due to the additional components or the switching losses with high the frequency operation.

This paper presents an active power decoupling circuit which is integrated to the CSI and the resonance type isolated DC/DC converter. The proposed converter compensates the instantaneous power fluctuation without large electrolytic capacitors. In addition, ZCS achieves at the all switching devices. Moreover, the large inductor is not required because the leakage inductance of the transformer is used as a DC inductor.

This paper is organized as follows: first, the configuration of the proposed circuit is shown. Next, the principle of the power decoupling control is described. In addition, the design method of the isolated DC/DC converter and its validity are explained with the simulation and experimental results. Finally, the fundamental operation and each evaluation are confirmed.

II. Circuit Topology

Fig. 1 shows the proposed converter which consists of a resonance-type isolated DC/DC converter, an active power decoupling circuit, and a CSI. The proposed converter does not need a large capacitor and inductor because the active power decoupling can be employed with a small buffer capacitor C_{buf}, and the proposed converter operates at the high switching frequency more than one-hundred kHz.

Firstly, the resonance-type isolated DC/DC converter achieves the ZCS operation using resonance with arm capacitors C_1, C_2 and leakage inductance of the transformer L_s. Note that, the switching frequency is set at the resonance frequency, and the primary side MOSFET S_1 and S_2 operates with 50% of switching duty. The resonance frequency is designed to be high in order to reduce the volume of the transformer.

The active power decoupling circuit compensates the power fluctuation with the small capacitor C_{buf} and rectifies the high frequency resonance current. After that, the high frequency rectified current flows to the single-phase AC grid or C_{buf}. In order to reduce the switching loss of the active power decoupling circuit and the CSI, the delta-sigma-based pulse density modulation (Δ–Σ_PDM) is applied instead of the pulse width modulation (PWM). Therefore, ZCS is achieved on the zero current point of the high frequency rectified current.

As shown in Fig. 1, the proposed converter requires many switching devices. The main contribution in this paper is the elimination of the large passive components in the circuit topology, e.g. the large inductor and costly. On the other hand, the cost of the switching devices may become cheap when the micro-inverter is massively adapted to the PV system.

III. Control Method

A. Principle of single-phase power fluctuation

Fig. 2 shows the principle of the active power decoupling. When both the output voltage and current waveforms are sinusoidal, the instantaneous output power p_{out} is expressed as

$$p_{out} = \frac{V_{acp} I_{acp}}{2}(1-\cos 2\omega t) \tag{1}$$

where, V_{acp} is the peak voltage, I_{acp} is the peak current, and ω is the angular frequency of the output voltage. As shown in (1), the power ripple that fluctuates at twice frequency of the AC grid occurs at DC link.

In order to absorb the power ripple, the instantaneous power p_{buf}, should be controlled as in (2)

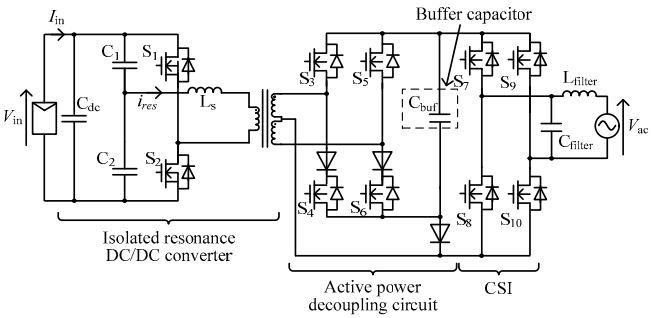

Fig. 1. Proposed DC to single-phase AC grid connected converter which is not required large energy buffer. The proposed converter achieves ZCS on each MOSFETs.

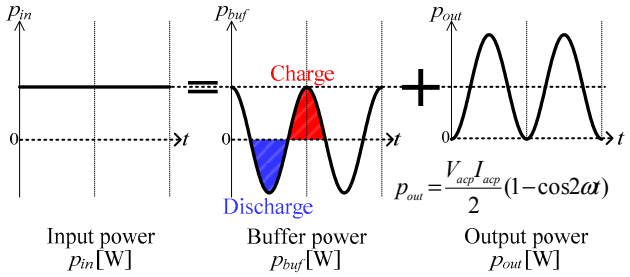

Fig. 2 Compensation principle of the single-phase power pulsation. Small buffer capacitor C_{buf} eliminates the second-order harmonics on P_{in}.

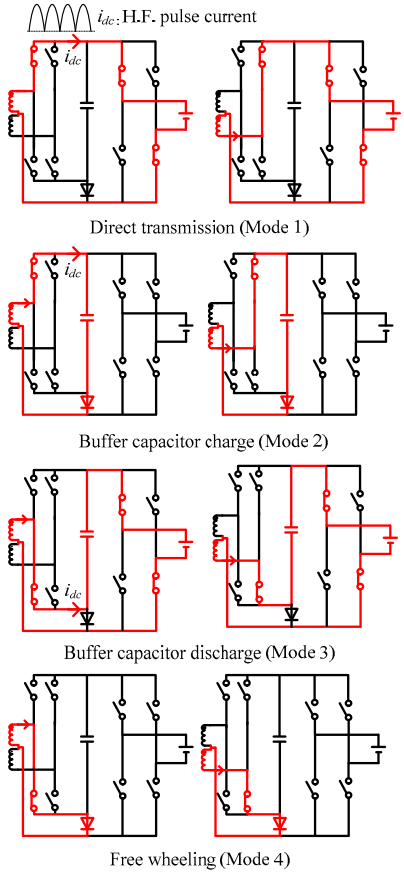

Fig.3 Operation mode of active buffer circuit and CSI. The buffer capacitor is charged and discharged by mode 2 and mode 3. Each mode is switched at the zero current point of the high frequency pulse current.

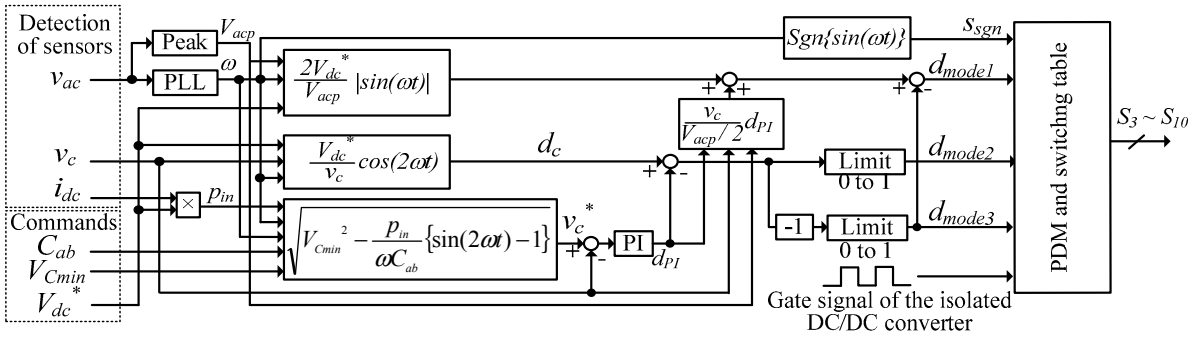

Fig. 4 Control block diagram of active power decoupling circuit and CSI.
In order to achieve ZCS, the delta-sigma-based pulse density modulation is applied.

$$p_{buf} = \frac{1}{2} V_{acp} I_{acp} \cos 2\omega t \tag{2}$$

where, the polarity of p_{buf}, is defined as positive when the flying capacitor C_{fc} discharges. Note that the active power of the flying capacitor C_{fc} is zero. Due to the power decoupling, the input power is matched to the output power. Thus, the relationship between the input and output power is expressed as

$$p_{in} = \frac{1}{2} V_{acp} I_{acp} = V_{IN} I_{IN} \tag{3}$$

B. Operation modes of active power decoupling circuit

Fig. 3 shows the operation mode of the active power decoupling circuit and the CSI when the grid voltage is the positive. Note that, the current pathway from the single-phase grid to the small capacitor C_{buf} does not occur because the capacitor voltage is always higher than the peak grid voltage. The active power decoupling circuit and the CSI are controlled in four modes defined by the switching pattern in Fig.4. In mode1, the input power P_{in} is directly supplied to the single-phase grid. In this control, the buffer power p_{buf} is controlled only by mode 2 and mode 3. In mode 2, the small capacitor C_{buf} is charged. In contrast, C_{buf} is discharged to the single-phase grid in mode 3. As a result, the small capacitor voltage is fluctuated at the twice frequency of the single-phase grid. Finally, mode 4 is the freewheeling mode.

In these modes, the active power decoupling circuit is switched in synchronization with the operation arm dependently on the resonance current polarity. Consequently, the CSI operates with the single-phase grid voltage according to the polarity of the resonance current.

C. Control block diagram of proposed circuit

Fig. 4 shows the control block diagram. The duty reference d_{mode1}, d_{mode2} and d_{mode3} are expressed as

$$d_{mode1} = 2\frac{V_{IN}^*}{V_{INp}}\left|\sin(\omega t)\right| - d_{mode3} \tag{4}$$

$$\begin{cases} d_{mode2} = \begin{cases} d_{tempo} & , d_c \geq 0 \\ 0 & , d_c \leq 0 \end{cases} \\ d_{mode3} = \begin{cases} -d_{tempo} & , d_c \leq 0 \\ 0 & , d_c \geq 0 \end{cases} \end{cases} \tag{5}$$

where, V_{dc}^* is the reference value of the input voltage of the active power decoupling circuit. d_c is the duty reference for the charge and discharge of the buffer capacitor C_3. On the other hand, the buffer capacitor current i_c is expressed as

$$i_c = \frac{V_{acp} I_{acp}}{2 v_c} \cos(2\omega t) \tag{6}$$

where, v_c is the instantaneous voltage of the buffer capacitor C_{buf}. In addition, i_c is decided by the d_{mode2}, d_{mode3}, and I_{dc}. The relationship between the duty references and i_c is expressed as

$$i_c = (-d_{mode2} + d_{mode3}) I_{dc} \tag{7}$$

According to (6) and (7), d_c is expressed as

$$d_c = \frac{V_{acp} I_{acp}}{2 v_c I_{dc}} \cos(2\omega t) = \frac{V_{dc}^*}{v_c} \cos(2\omega t) \tag{8}$$

where, V_{dc}^* has to be satisfied as in the following condition

$$V_{dc}^* \leq \frac{V_{acp}}{2} \tag{9}$$

This is because the all duty commands should be positive.

In this control, the buffer capacitor voltage control (AVR) is operated to compensate the error between the duty references and the actual voltage. Note that the phase reference is synchronized to the single-phase AC grid voltage by Phase Looked Loop (PLL).

D. *Modulation method of proposed converter*

Fig. 5 shows the modulation block diagram of the Δ–Σ_PDM. The duty command values d_{mode1} to d_{mode3} are converted to the selector signal $Sel_{\_mode1}$ to $Sel_{\_mode3}$ for each operation mode. First, the error between each duty command and the selector signal are calculated, and integrated. Next, the quantize outputs $Sel_{\_mode1}$ to $Sel_{\_mode3}$ corresponding to the integral error. Note that, quantizes are operated with the quantizing clock (CLK_Q), and CLK_Q is synchronized with the zero current point of the pulse current. CLK_Q is obtained by the gate signals of the primary MOSFET because when the transformer power factor is unity, the zero current point varies corresponding to the primary transformer current zero cross point. Appling Δ–Σ_PDM, the active power decoupling circuit and the CSI achieve the ZCS operation because each MOSFET is switched at the zero current point of the secondary-side input current.

The secondary input current is supplied from the isolated resonance DC/DC converter to the active power decoupling circuit and the CSI. Note that ZCS is achieved based on this current. Thus, the design of the resonance parameter is important for proposed operation.

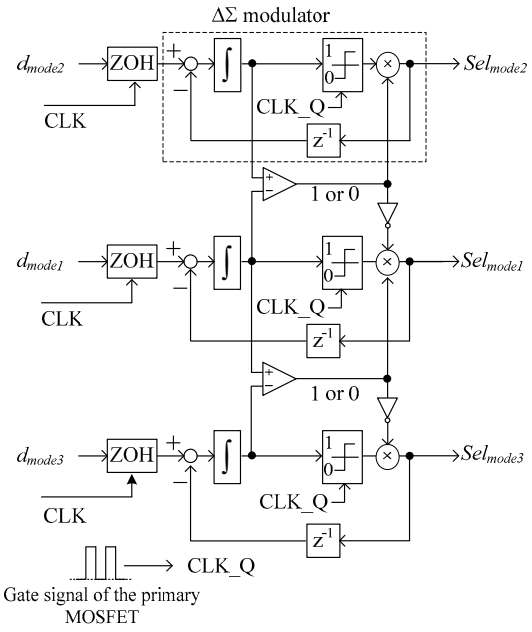

Fig. 5 Modulation block diagram of delta-sigma based pulse density modulation.

IV. Design Method of Isolated Resonance DC/DC Converter

A. *Fundamental design*

Fig. 6 (a) shows the equivalent series resonance model of the isolated DC/DC converter. In this model, the smoothing capacitor is connected on the rectifier output part in order to eliminate the switching frequency component. In this case, the arm capacitor C_1, C_2 and the leakage inductance of the transformer L_s are utilized for the series resonance, and the isolated DC/DC converter achieves the ZCS operation. Generally, the transformer voltage results in the square waveforms, and the transformer peak voltage is always the half of the PV input voltage V_{in}.

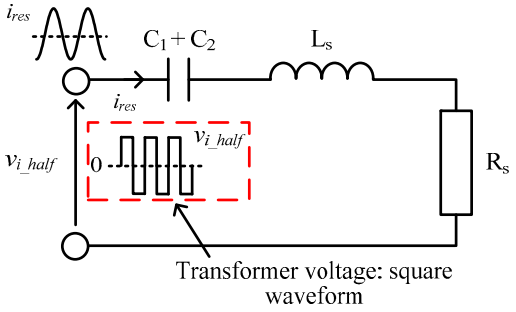

(a) Ideal model for series resonance.

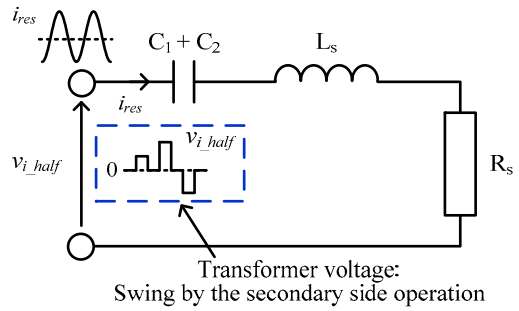

(b) Series resonance model of proposed circuit.

Fig. 6 Equivalent model of series resonance for isolated DC/DC converter.

Fig. 6 (b) shows the equivalent model for the proposed converter. The proposed converter does not adopted the switching filter between the isolated DC/DC converter and the active power decoupling circuit because the high frequency resonance current is utilized for the ZCS operation with the active power decoupling circuit and the CSI. However, when the smoothing capacitor is not adopted, the operation of the secondary converter interferes to the resonance condition. As a result, the transformer peak voltage fluctuates depending on the operation mode as shown in Fig.3. Due to this reason, the conventional resonance parameter design cannot be applied for the proposed converter. In this chapter, a design criterion of the resonance parameters is considered.

Firstly, the resonance frequency f_{res} is expressed as

$$f_{res} = \frac{1}{2\pi\sqrt{(C_1 + C_2)L_s}} \qquad (10)$$

where, the resonance frequency is designed as the high frequency more than the one-hundred kHz in order to reduce the volume of the transformer. When the switching frequency and the resonance frequency becomes the same, the resonance current i_{res} becomes sinusoidal. The peak resonance current I_{res} is expressed as

$$I_{res} = \frac{4}{\pi}\frac{V_{i\_half}}{R_s} \tag{11}$$

where, V_{i_half} is the primary-sides peak voltage of the transformer, R_s is the equivalent AC resistance. In this case, R_s is expressed as

$$R_s = \frac{8}{\pi^2}\left(\frac{N_1}{N_2}\right)^2 \frac{V_{in}}{I_{in}} \tag{12}$$

Finally, the resonance peak current I_{res} is derived from (10) and (11)

$$I_{res} = \pi I_{in} \tag{13}$$

B. Determination of LC resonance parameters

When the resonance parameters C_1, C_2 and L_s are selected based on the resonance frequency, many options exists. One of the criterion is the quality factor Q, and it influences to the resonance frequency characteristics.

The quality factor Q of the series resonance is expressed as

$$Q = \frac{1}{R_s}\sqrt{\frac{L_s}{C_1 + C_2}} \tag{14}$$

Fig. 7 shows the resonance frequency characteristics when the Q value is changed. As shown in Fig.7, the resonance peak current at the resonance frequency is the same with both the low Q and high Q values.

On the other hand, the resonance voltage is proportional to the Q value. The resonance peak inductor voltage V_{Lpeak} is expressed as

$$V_{Lpeak} = QR_s I_{res} \tag{15}$$

When the resonance parameters is designed at the high Q value, the resonance voltage on each resonance condition becomes large. Thus, each component is required the high rated voltage.

When the series resonance is designed to focus on the high efficiency, the Q value should be low. Because in the low Q design, the leakage inductance and the resonance peak voltage can be small from (14) and (15). However, when the Q value is design to low, the resonance current peak oscillates due to the disturbance. The damping coefficient ξ is expressed as

$$\xi = \frac{1}{2Q} \tag{16}$$

When ξ is high, the resonance current fluctuates unstably, and it is difficult to sustain the continuity of the series resonance. Especially, the proposed circuit does not use the switching filter between the isolated resonance DC/DC converter and the secondary-side converter. Thus, secondary-side converter operation interferes the resonance condition as the disturbance. As a result, the resonance current decays.

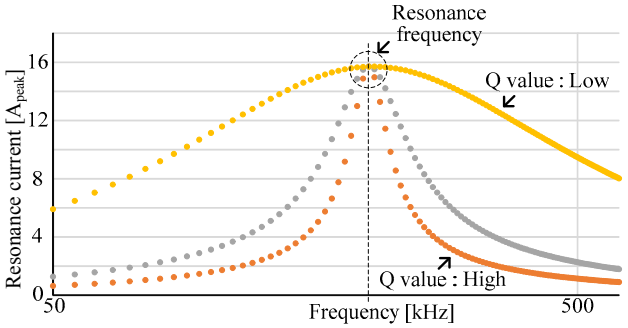

Fig. 7 Characteristics of series resonance current. When the equivalent AC resistance is same, the resonance current peak become maximum at the resonance frequency.

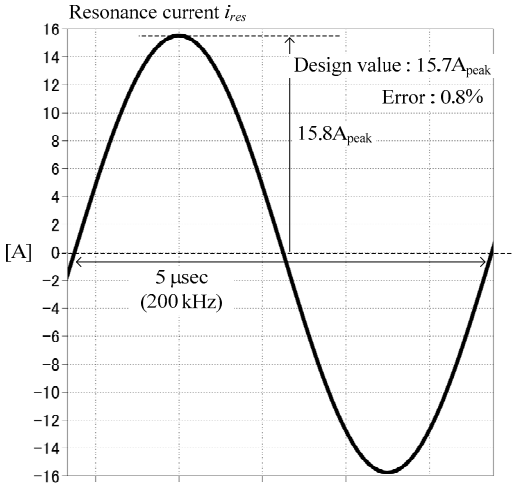

Fig. 8 Simulation result of resonance current. The error between the design and the simulation value is less than 1%.

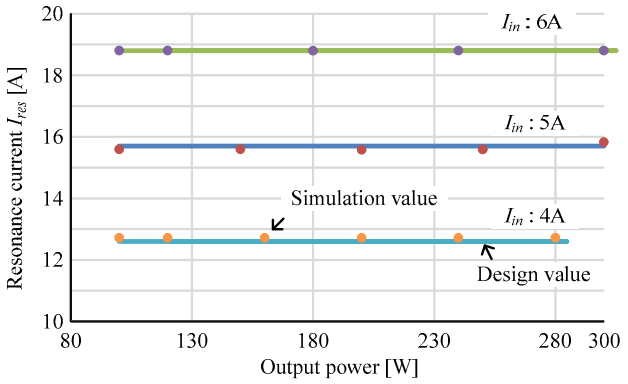

Fig. 9 Comparison between resonance current and design value when output power and input current is changed.

In order to consider the resonance condition on the proposed converter, two conditions are simulated in next chapter. One is the low Q value condition, and it is confirmed that the error between the simulation and the design value becomes large. On the other hand, in the high Q condition, the simulation value agrees with the design value.

V. EVALUATION OF RESONANCE PARAMETER DESIGN

A. Simulation results

Fig. 8 shows the simulation result of the proposed resonance design. In this simulation, the Q value is designed to be high value, and the resonance frequency is set at 200 kHz. As shown in Fig.8, the error between the design value and the simulation value is less than 1%, and the resonance current becomes a sinusoidal waveforms.

Fig. 9 shows the relationship between the output power and the resonance peak current. In this result, the input current condition is changed from 4 A to 6 A. According to Fig. 9, all the simulation results agree with the design values at the condition of the high Q value. However, when the Q value is low, the error between the design value and the simulation result becomes large.

Fig. 10 shows the simulation result with different Q values. In the Fig. 10 (a), the resonance parameters are designed at the low Q condition. In addition, the resonance peak current is designed to be 15.7A. According to Fig. 10 (a), the maximum error between the simulation value and the design value is 52% at the condition of the low Q value.

On the other hand, with the condition of the high Q value in Fig.10 (b), the error is reduced by 99% in comparison with Fig. 10(a). It is because the transformer peak voltage is fluctuated in the proposed converter.

The reason why the high error between the simulation value and the design value occurs at the low Q value is explained as following. The proposed converter does not adopt the switching filter on the DC bus, and the resonance current is utilized to achieve ZCS for the active power decoupling circuit and the CSI. Thus, the secondary-side peak voltage of the transformer fluctuates. For example, in mode 2, the secondary-side resonance current flows in the small capacitor C_{buf}, and the secondary-side voltage of the transformer is clamped to the small capacitor voltage V_{cbuf}. On the other hand, in the mode1, the resonance current is supplied to the single-phase grid. As a result, the secondary transformer voltage is clamped to the grid voltage V_{ac}. When the Q value is low, the resonance peak current is fluctuated severely. This is because the series resonance is excited by the transformer voltage. However, the same resonance peak current at the all switching mode is preferable. In order to suppress the resonance peak current fluctuation, the Q value should be high. This leads to the low damping coefficient ξ which can sustain the series resonance. Following these results, when the resonance current is required to agree with the design value, the Q value of the series resonance has to become high.

B. Experimental result of the resonance current design

In order to validity of the proposed design method, two 300W prototype circuits are tested. Table. 1 shows the experimental parameters. In this experiment, two conditions for the type isolated resonance DC/DC converter are evaluated. The only difference between the two converters is the resonance parameter. Therefore, the same switching device, transformer cores, windings are selected. Note that, the winding structure is different in order to adjust the leakage inductance. When the Q

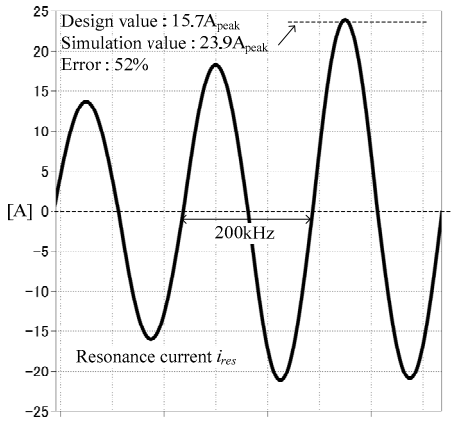

(a) L_{res} : 20μH, C : 30nF, Q : 11.

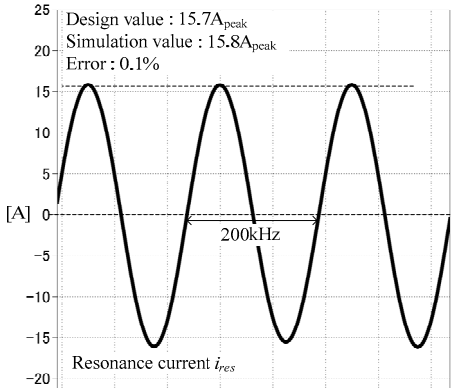

(b) L_{res} : 200μH, C : 3nF, Q : 109.

Fig. 10 Resonance current when Q value is changed. When the condition of the low Q value is employed, the error between the design value and the simulation value becomes large.

Table.1 Experimental parameters

Input voltage	V_{in}	90 V
Input current	I_{in}	3.5 A
Output power	P_{out}	300 W
Switching freq.	f_{sw}	150 kHz
Resonance freq.	f_{res}	150 kHz
Turn ratio	N_1:N_2	1:2
Resonance Parameters	High Q Low Q	L_s:13μH C : 0.1μF L_s:800nH C : 1.2μF

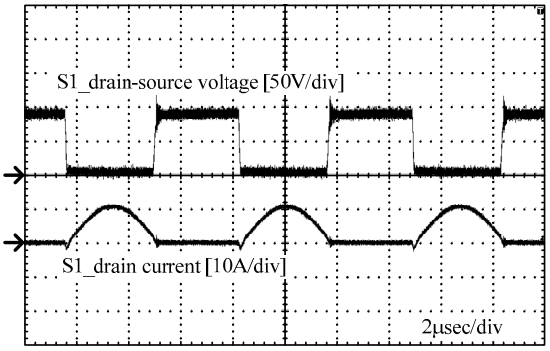

Fig. 11 Experimental result with ZCS of isolated resonance DC/DC converter.

value is to be high, the leakage inductance is large. In addition, the resonance frequency is designed to 150 kHz.

Fig. 11 shows the primary MOSFET switching waveforms. According to fig.11, the drain-source voltage of S_1 is switched at the zero current point, e.g. the achievement of ZCS. Note that, ZCS is achieved in both the high Q condition.

Fig. 12 shows the comparison with the resonance peak current and the design value. Note that, the design value is calculated by (13). As shown in fig.13, the maximum error is 4.5% when the input current is 3.5 A. Furthermore, the resonance current peak is increases proportionally to the input current. Note that, when ZCS is achieved, the reduction of the conduction loss of the each MOSFET is important for the achievement of the high efficiency. In this application, the primary side current of the transformer is large due to the low voltage condition. Thus, the full bridge type isolated DC/DC converter is better at the low voltage condition.

Fig. 13 shows the efficiency characteristics in both the high Q condition and the low Q condition. The maximum efficiency with the low Q value condition is 96.5%. On the other hand, the maximum efficiency with the high Q value is reduced by 2.9%. This is because the transformer loss increases. When the leakage inductance becomes large, the coupling coefficient of the transformer decreases. In addition, the resonance peak voltage becomes large in comparison with the low Q. as a result, the iron loss becomes large. Thus, the resonance inductor loss reduction is important in order to achieve the high efficiency. Therefore, the improvement of the converter efficiency with the high Q value has to be considered. This result is obtained with the half bridge isolated DC/DC converter, and the conduction loss is large because the transformer voltage becomes half. In order to improve the efficiency, the full bridge isolated DC/DC converter will be considered.

VI. Fundamental Evaluation of Proposed Circuit

Table 2 shows the simulation condition. Fig.14 shows the simulation result of the proposed circuit. According to fig. 14, it is confirmed that the buffer capacitor voltage is fluctuated at the twice grid frequency, and the input voltage ripple is under than 5% by controlling the buffer power p_{buf}. Thus, the operation of the power ripple compensation is achieved. In addition, the output power factor is almost unity at the rated power, and the output current THD is 2.3%. From these results, it can be confirmed that the proposed converter realizes the power decoupling with the small capacitor C_{buf}.

Fig. 15 shows the switching waveforms of the proposed circuit. Each MOSFET of the active buffer and the CSI are also switched at the zero current point by Δ–Σ_PDM. In addition, the isolated DC/DC converter achieves ZCS by the series resonance operation as shown in fig. 11. It can be concluded from these results that, the switching losses is drastically reduced.

In order to further improve the efficiency, the transformer design and the reduction of the conduction loss is important because the proposed converter has many MOSFETs, and the transformer losses such as the iron loss and the copper loss are large. The converter loss will be evaluated for high efficiency by experiment.

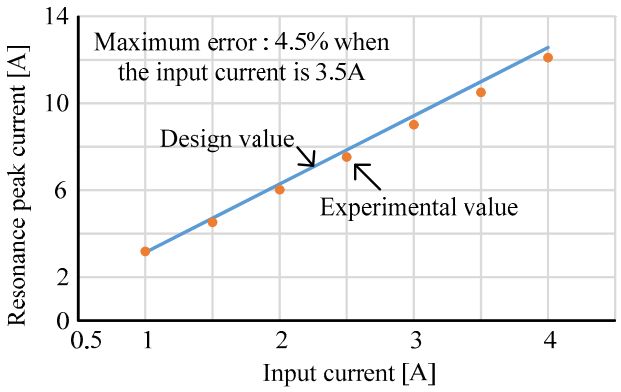

Fig. 12 Comparison between design value and experimental result. The experimental result agrees with the design value.

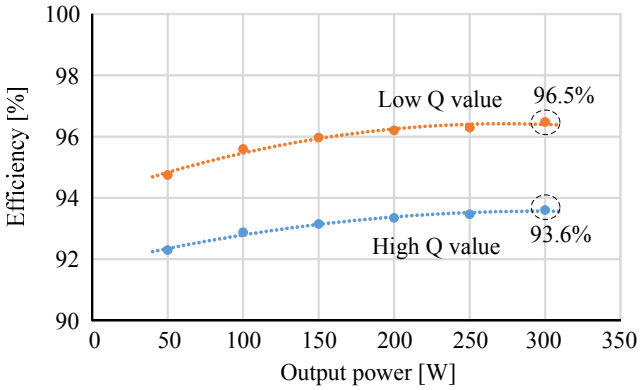

Fig. 13 Efficiency characteristics with isolated DC/DC converter when Q value is changed. In the high Q condition, the efficiency is reduced to 93.6%. This is because the transformer loss is large.

Table.2 Simulation parameter

Input voltage	V_{in}	60 V
Input current	I_{in}	5 A
Grid voltage	v_{ac}	200 V_{rms}
Grid frequency	f_{ac}	50 Hz
Output power	P_{out}	300 W
Switching frequency	$f_{sw\_primary}$	200 kHz
Trans turn ratio	$N_1 : N_2$	1 : 6 turn
Buffer capacitor	C_{buf}	50 μF
Quantizing clock	CLK_Q	400 kHz
Duty command updating cycle	CLK	48 kHz

VII. Conclusion

This paper presented the active power decoupling circuit which is integrated to the CSI and the resonance type isolated DC/DC converter. This converter compensated for the instantaneous power fluctuation without the large electrolytic capacitor. In addition, ZCS is achieved at the all switching devices and the large inductor are not required because the leakage inductance of the transformer is used as a DC inductor.

The power decoupling with the small capacitor and the high frequency operation was employed. Moreover, the clarification

of resonance parameter design for the proposed converter was conducted. As a result, the experimental resonance current peak is agrees with the design value with the error is less than 5%. In the proposed converter, the quality factor Q of the series resonance should be designed to be high in order to maintain the stability of the resonance current. In this case, the reduction of the resonance inductor loss is important in order to achieve the high efficiency. Finally, the fundamental operation of the proposed converter was confirmed by simulation. As a result, the input voltage ripple was suppressed under than 5% by the power decoupling control with small capacitor.

In the future work, the proposed converter operation will be evaluated by the experiment. In addition, each loss and the high efficiency design will be considered.

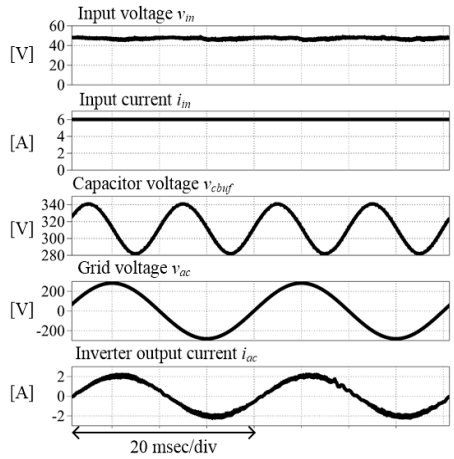

Fig. 14 Simulation result with the proposed converter. The input voltage become constant by active power decoupling.

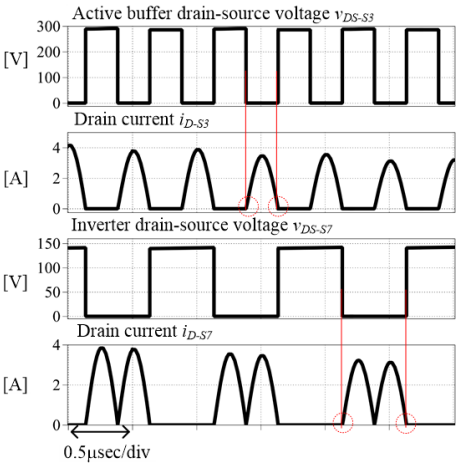

Fig. 15 Each switching waveforms applying the ZCS. The proposed converter can achieve the ZCS including the isolated resonance DC/DC converter.

REFERENCES

[1] S-M.Tayebi, X. Mu, I. Batarseh: "Improved three-phase micro-inverter using dynamic dead time optimization and phase-skipping control techniques", IEEE Applied Power Electronics Conference and Exposition (APEC), pp.1381-1386,(2016)

[2] X. Liu, M. Agamy, D. Dong,M. Harfman-Todorovic, L-Garces: "A low-cost solar micro-inverter with soft-switching capability utilizing circulating current", IEEE Applied Power Electronics Conference and Exposition (APEC), pp.3403-3408,(2016)

[3] N. Pragallapati, T. Lodh, V. Agarwal: "Parallel-input series-output interleaved flyback based solar PV module integrated micro-inverter", International Conference on Renewable Energy Research and Application (ICRERA), pp.716-720,(2015)

[4] F. Ji, L. Mu, G. Zhu: "A novel Multi-function photovoltaic Micro-inverter and its control strategy", IEEE 8th International Power Electronics and Motion Control Conference (IPEMC-ECCE Asia), pp.1302-1305,(2016)

[5] E. Fonkwe, J. Kirtley, J. Elizondo: "Elyback micro-inverter with reactive power support capability", IEEE 17th Workshop on Control and Modeling for Power Electronics (COMPEL), pp.1-8,(2016)

[6] H. Renaudineau, S. Kouro, K. Schaible and M. Zehelein: "Flyback-based Sub Module PV Microinverter", EPE`16 ECCE Europe, (2016)

[7] R-K. Surapaneni, A-K. Rathore: "A novel single-phase isolated PWM half-bridge microinverter for solar photovoltaic modules", ECCE US pp. 4550-4556 (2015)

[8] T. Boutot and L. Chang, "Development of a single-phase inverter for small wind turbins," in Proc. IEEE Electrical and Computer Engineering Canadien Conf. (CCECE'98), pp. 305-308 (1998)

[9] Y. Xue, L. Chang, S. B. Kjaer, Bau, J. Bordonau, T. Shimizu, "Topologies of Single-phase Inverters for Small Distributed Power Generators: An Overview," IEEE Transactions on Power Electronics, Vol.19, No.5, pp. 1305-1314 (2004)

[10] H. Hu, S. Harb, N. Kutkut, I. Batarseh, Z. J. Shen, "Power Decoupling Techniques for Micro-inverters in PV Systems — a Review," Energy Conversion Congress and Exposition 2010, pp.3235-3240, pp. 12-16 (2010)

[11] T. Shimizu, K. Wada, N. Nakamura: "Flyback-Type Single-Phase Utility Interactive Inverter With Power Pulsation Decoupling on the DC Input for an AC Photovoltaic Module System", IEEE Trans., Vol. 21, No. 5, pp. 1264-1272 (2006)

[12] K. Kusaka, H. Watanabe, K. Furukawa, J. Itoh: "Power Decoupling Circuit with Flying Capacitor DC-DC Converter", JIASC2015, Vol. , No. 1-78, pp. (2015)

[13] F. Schimpf, L. Norum: "Effective Use of Film Capacitors in Single-Phase PV-inverters by Active Power Decoupling", IECON 2010, Vol. , No. , pp. 2784-2789 (2010)

[14] Kuo-Hen Chao, Po-Tai Cheng : "Power decoupling methods for single-phase three-poles AC/DC converters " ECCE 2009, pp3742-3747,(2009)

[15] Ruxi Wang, F.Wang, Rixin Lai, Puqi Ning, R.Burgos, D.Boroyevich : " Study of Energy Storage Capacitor Reduction for Single Phase PWM Rectifier " APEC 2009, pp1177-1183,(2009)

[16] Chaia-Tse Lee, Yen-Ming Chen, Li-Chung Chen, Po-Tai Cheng: "Efficiency Improvement of a DC/AC Converter with the Power Decoupling Capability"、IEEE APEC 2012 Vol. , No. , pp. 1462-1468 (2012)

[17] Y. Ohnuma, J. Itoh: "A Single-Phase Current-Source PV Inverter With Power Decoupling Capability Using an Active Buffer", , Vol. 51, No. 1, pp. 531-538 (2015)